Advanced Powder Technology 31 (2020) 954–966

Contents lists available at ScienceDirect

Advanced Powder Technology

journal homepage: www.elsevier.com/locate/apt

Original Research Paper

Unsteady natural convection flow of a suspension comprising Nano-Encapsulated Phase Change Materials (NEPCMs) in a porous medium

Mohammad Ghalambaz [a,b,*], S.A.M. Mehryan [c], Ahmad Hajjar [d], Ali Veismoradi [e]

[a] Department for Management of Science and Technology Development, Ton Duc Thang University, Ho Chi Minh City, Viet Nam
[b] Faculty of Applied Sciences, Ton Duc Thang University, Ho Chi Minh City, Viet Nam
[c] Young Researchers and Elite Club, Yasooj Branch, Islamic Azad University, Yasooj, Iran
[d] ECAM Lyon, LabECAM, Université de Lyon, Lyon, France
[e] Chemical Engineering Department, Ferdowsi University, Mashhad, Iran

ARTICLE INFO

Article history:
Received 20 September 2019
Received in revised form 26 November 2019
Accepted 9 December 2019
Available online 27 December 2019

Keywords:
Nano-Encapsulated Phase Change Materials (NEPCMs)
Porous medium
Heat transfer enhancement
Unsteady natural convection

ABSTRACT

The free convection phase change heat transfer of a suspension comprising Nano-Encapsulated Phase Change Materials (NEPCMs) in a porous space is theoretically addressed. The core of the nanoparticles is made of a phase change material and encapsulated in a thin shell. Hence, the core of the nanoparticles of the suspension undergoes a phase change at its fusion temperature and release/store large amounts of latent heat. The phase change of nanoparticles is modeled using a sine shape temperature-dependent heat capacity function. Darcy-Brinkman model is used to model the flow in the porous medium. The governing equations including the conservation of mass, momentum, and heat are transformed into a non-dimensional form before being solved by the finite element method in a structured non-uniform mesh. The influence of the porosity, Darcy number, Rayleigh number, fusion temperature of nanoparticles, and the unsteady time-periodic boundary conditions on the thermal behavior of the porous medium in the presence of NEPCM particles is investigated. The results show that the presence of NEPCM particles improves the heat transfer. The increase of porosity improves the heat transfer when the volumetric concentrations of NEPCM particles are higher than 3%. There exists an optimal dimensionless fusion temperature of NEPCM nanoparticles for the interval [0.25; 0.75].

1. Introduction

The study of convective heat transfer in porous media is of fundamental importance in various engineering and industrial fields. Common applications include geothermal systems, energy storage, heat exchangers, thermal insulation, drying technologies, and the list goes on. The presence of porous media in the system enhances heat transfer as it affects the flow field and increases the effective thermal conductivity, and it presents, thus, a passive technique of heat transfer improvement.

Free convection in cavities filled with porous media has been widely analyzed for different cavity models including cavities filled with single or multiple layers of porous media [1–3], porous fins [4], partially porous media [5,6], tilted cavities [7], wavy cavities [8] and cavities with non-uniform heating [9]. Convective flows past a vertical plate embedded in a porous medium have been also considered [10–12].

Further heat transfer enhancement can be obtained by adding highly conductive nanoparticles into the fluid flowing through the porous medium [13]. The fluid is thus called a nanofluid. Several works aimed to study the free convection of nanofluids in various types of enclosures [14–17], two-phase flow of nanofluids [16,18], conjugate heat transfer [19,20], entropy generation [21,22], and magnetic fields effects [18,21,23–26]. Moreover, convective flows of nanofluids in cavities with porous media have been widely investigated considering various designs and configurations, including internal heat generation [27,28], thermal non-equilibrium effects [29], partial porous layer [30,31]. The shape effects of the nanoparticles on the heat transfer characteristics have been also considered [32–34].

Nano-Encapsulated Phase Change Materials (NEPCM) suspensions represent a class of Nanofluids where the nanoparticles consist of capsules having a shell-core structure, with phase change

* Corresponding author at: Ton Duc Thang University, Ho Chi Minh City, Viet Nam.
E-mail addresses: mohammad.ghalambaz@tdtu.edu.vn (M. Ghalambaz), alal171366244@gmail.com (S.A.M. Mehryan), ahmad.hajjar@ecam.fr (A. Hajjar), ali.veismoradi@mail.um.ac.ir (A. Veismoradi).

https://doi.org/10.1016/j.apt.2019.12.010
0921-8831/

Nomenclature

Latin letters

a	the amplitude of temperature fluctuation
A	Non-dimensional amplitude
C_p	the specific heat (J/kg·K)
Cr	the ratio of the heat capacity of the suspension to the host fluid
Da	Darcy number
f	the non-dimensional form of phase change profile
g	the gravity constant (m/s^2)
H	the characteristic length, cavity size
h_{sf}	the latent heat of the nanoparticle's core
i	Grid case number
k	the coefficient of the thermal conductivity (W/m K)
K	the porous medium permeability (m^2)
N	the mesh size
Nc	the conductivity number for the suspension
Nu	Nusselt number
Nv	the dynamic viscosity number for the suspension
p	the suspension pressure field (Pa)
P	non-dimensional the suspension pressure field
Pr	Prandtl number
Ra	Rayleigh number
Ste	Stefan number
t	time (s)
T	the temperature (°C)
T_{Mr}	the melting temperature range
u	the fluid velocity along x axis (m/s)
U	dimensionless fluid velocity along x axis
v	fluid velocity along y axis (m/s)
V	the dimensionless fluid velocity along y axis
x	x-Cartesian coordinate (m)
X	dimensionless X-Cartesian
y	y-Cartesian coordinate (m)
Y	dimensionless Y-Cartesian coordinate
ι	the weight ratio of the NEPCM particle's core to shell

Greek symbols

μ	the dynamic viscosity of the fluid (kg s/m)
α	the thermal diffusivity (m^2/s)
β	the coefficient of the volumetric thermal expansion (1/K)
Δ	the relative error of the computations
δ	the dimensionless phase change band
ε	the porosity of the medium
θ	the non-dimensional temperature field
λ	the dimensionless ratio of the heat capacity
ρ	density (kg/m^3)
τ	non-dimensional time
ϕ	the volume fraction of particles in the host fluid
ψ	the stream function
ω	the angular frequency of the wall temperature oscillation (rad/s)
Ω	the non-dimensional angular frequency of the wall temperature oscillation

Subscript

b	the NEPCM suspension
c	the cold wall
co	the core of encapsulated particles
f	the host fluid
fu	the fusion property
h	the hot wall
m	the porous medium
p	the NEPCM nanoparticles, period
s	the solid matrix of the porous medium
sh	the shell of NEPCM particle

materials (PCM) at the core. PCM are materials that undergo a phase change at their fusion temperature. They can thus absorb heat from the surrounding by melting, or, conversely, release heat by solidification. The presence of NEPCM capsules in the host fluid can enhance substantially its thermal conductivity. For instance, [35] showed that adding NEPCM particles with a volume fraction as low as 3.36% can increase the thermal conductivity of water by 20%. A distinction should be made between nano-encapsulation and micro-encapsulation depending on the size of the particles [36,37]. The term nanoparticle is often used when the size of the particle is less than 100 nm in at least one dimension. PCM cores are selected based on the required fusion temperature. Examples of PCM that have been used as NEPCM cores include n-tetradecane [38], n-octadecane [39], n-octacosane [40], and n-nonadecane [35]. On the other hand, the shell of the NEPCM capsules can be made of polymers of different compositions [41,42], formaldehyde [38,39] or highly conductive metals [40]. There is a technique that consists of adding nanoparticles to PCM in order to improve heat transfer [43], leading to the so-called Nano-Enhanced Phase Change Materials, also abbreviated as NEPCM [43–45]. It should be noted that this technique is different than the one studied in the present paper.

Convective flows of PCM in enclosures with porous media have been widely studied, mainly in the context of heat transfer enhancement by the use of metal foams [46–49]. As for NEPCM suspensions, the majority of available works dealt with the forced convection in tubes or mini channels. Ho et al. [50–52] investigated experimentally the effectiveness of using water-based suspensions of Alumina nanoparticles and/or micro-encapsulated PCM instead of pure water on the forced convection in circular tubes [50] and mini channel heat sinks [51,52]. They found that different factors, such as the flow rate and the heating location can considerably affect the heat transfer in the system. The analysis of the heat transfer enhancement in microtubes using PCM nano-encapsulation was performed by Seyf et al. [53]. Their results indicated that using a higher concentration of the NEPCM particles significantly increased the cooling power of the fluid, despite leading to a larger pressure drop in the tube. A similar result was obtained in the numerical study of a NEPCM slurry heat transfer past an unconfined square cylinder performed by [54], who pointed out a noticeable haet transfer enhancement in the slurry compared to the base fluid, and an intensification of this enhancement when the volume concentration of the capsules was increased.

On the other side, the free convective flow of NEPCM suspensions did not receive much attention. Ghalambaz et al. [55] investigated the natural convective flow of a NEPCM suspension in a square cavity with temperature difference between the two vertical walls and thermal insulation on the horizontal walls. They concluded that the fusion temperature of the phase change core is a fundamental parameter in the heat transfer inside the cavity. Moreover, studies considering the free convection of NEPCM in porous cavities are very limited. In fact, the available studies linking capsulated PCM to porous media focused on the enhancement of the thermal properties of some construction materials by using NEPCM as nano additives composites [56,57] without any convection effects.

Very recently, Ghalambaz et al. [58] conducted a study on the influence of using NEPCMs suspensions in the mixed convection boundary layer flow over a flat plate embedded in a saturated porous medium. They utilized the boundary layer approximations and reduced the model to ordinary differential equations and investigated the effect of volume fraction of nanoparticles on the boundary layer flow and heat transfer. They found that further enhancement of heat transfer can be achieved by decreasing the fusion temperature of the NEPCM core.

Therefore the literature studies regarding the convection heat transfer of NEPCMs are limited to steady-state convection in a clear cavity with no porous medium [55], and steady-state mixed convection boundary layer of NECPMs in an infinite layer of porous medium [58]. Following [55,58], the present study aims to analyze the unsteady free convection of a suspension of NEPCMs in a cavity filled with a porous medium for the first time. The unsteady effects are expected to be important due to the presence of phase change heat transfer phenomena in the nanoparticle's cores.

2. Mathematical model

2.1. Model description

The geometry consists in a 2D square enclosure (demonstrated in Fig. 1), containing glass balls, saturated with a suspension of water and NEPCM particles. The shell and core of the NEPCM are respectively polyurethane (PU) and nonadecane. As shown in Fig. 1, the left of the medium is imposed to a high time-varying temperature having the average temperature of T_h. The opposite wall is a heat sink at the lower temperature T_c while the top and bottom walls of the enclosure are thermally impervious. The flow in the porous space is described using Darcy-Brinkman model. There are no thermal and hydrodynamic slips along the fluid and the nanoparticles, and the particles are uniformly dispersed in the suspension. Moreover, there exists a strong heat transfer between the solid matrix and fluid phase of the porous medium. Indeed, the local thermal equilibrium condition is established between these two components. Table 1 lists the thermophysical properties of the involved materials. Also, the phase change temperature and the latent heat of the NEPCMs core are respectively 32 °C and 211 kJ/kg [35]. It should be noted that the materials are optional, and the present study is not restricted to the mentioned type of materials.

2.2. The governing equations

Considering the assumptions, the unsteady equations modeling thermal and hydro-dynamic behaviors of an incompressible and laminar suspension inside a porous region are listed below:

Mass conservation [55]:

$$\frac{\partial u}{\partial x}+\frac{\partial v}{\partial y}=0 \tag{1}$$

Momentum conservation [60–62]:

$$\frac{\rho_b}{\varepsilon}\frac{\partial u}{\partial t}+\frac{\rho_b}{\varepsilon^2}\left(u\frac{\partial u}{\partial x}+v\frac{\partial u}{\partial y}\right)=-\frac{\partial p}{\partial x}+\frac{\mu_b}{\varepsilon}\left(\frac{\partial^2 u}{\partial x^2}+\frac{\partial^2 u}{\partial y^2}\right)-\frac{\mu_b}{K}u \tag{2a}$$

$$\frac{\rho_b}{\varepsilon}\frac{\partial v}{\partial t}+\frac{\rho_b}{\varepsilon^2}\left(u\frac{\partial v}{\partial x}+v\frac{\partial v}{\partial y}\right)=-\frac{\partial p}{\partial y}+\frac{\mu_b}{\varepsilon}\left(\frac{\partial^2 v}{\partial x^2}+\frac{\partial^2 v}{\partial y^2}\right)+g\rho_b\beta_b(T-T_c)-\frac{\mu_b}{K}v \tag{2b}$$

Energy conservation [60,62]:

$$(\rho C_p)_{m,\,b}\frac{\partial T}{\partial t}+(\rho C_p)_b\left(u\frac{\partial T}{\partial x}+v\frac{\partial T}{\partial y}\right)=k_{m,\,b}\left(\frac{\partial^2 T}{\partial x^2}+\frac{\partial^2 T}{\partial y^2}\right) \tag{3}$$

where [63]

$$k_{m,b}=(1-\varepsilon)k_s+\varepsilon k_b \tag{4a}$$

$$(\rho C_p)_{m,b}=(1-\varepsilon)(\rho C_p)_s+\varepsilon(\rho C_p)_b \tag{4b}$$

The subscripts of b, m, and s of the above-written equations explain the bulk properties of the suspension, porous medium, and solid matrix, respectively. Regarding the problem physics, the boundary conditions are:

$$x=0,\ 0\leqslant y\leqslant H:\quad u=v=0,\ T=T_h+a\sin(\omega t) \tag{5a}$$

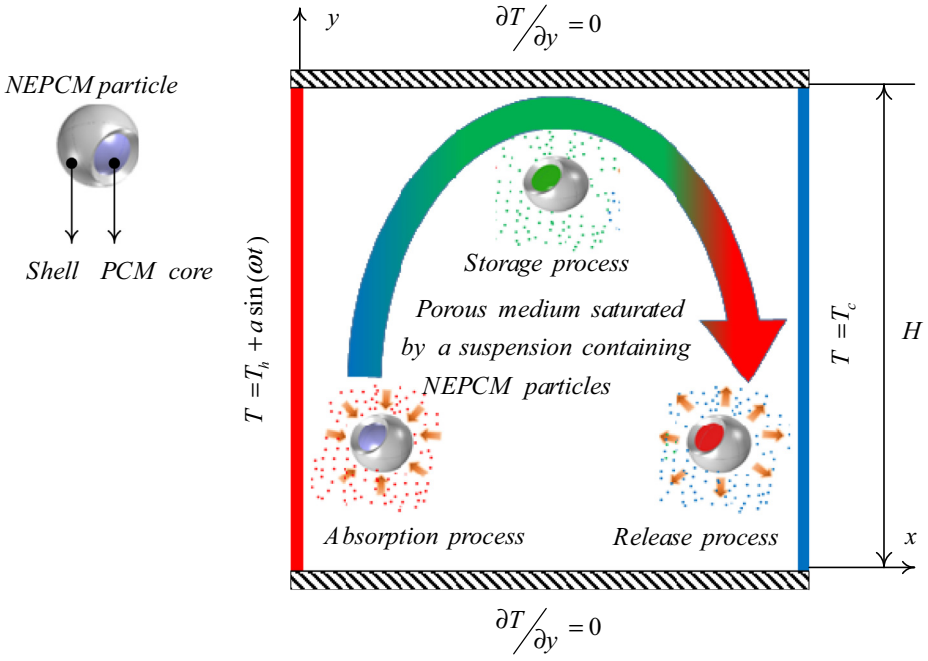

Fig. 1. Schematic configuration of the physical model.

Table 1
Thermophysical properties of the involved material in the problem [35,59]

	C_p (KJ/Kg·K)	μ (kg/m·s)	k (W/m·K)	ρ (Kg/m^3)	β (K^{-1})
Host fluid	4179	8.9×10^{-4}	0.613	997.1	21×10^{-5}
PU	1317.7	–	–	786	17.28×10^{-5}
Nonadecane	2037	–	–	721	–
Glass balls	840	–	1.05	2700	0.9×10^{-5}

$$x = H,\ 0 \leqslant y \leqslant H\ :\quad u = v = 0,\ T = T_c \tag{5b}$$

$$\begin{aligned} y = H,\ 0 \leqslant x \leqslant H:&\quad u = v = 0\ ,\frac{\partial T}{\partial y} = 0 \\ y = 0,\ 0 \leqslant x \leqslant H:&\quad u = v = 0\ ,\frac{\partial T}{\partial y} = 0 \end{aligned} \tag{5c}$$

2.3. Bulk thermophysical properties of the NEPCM suspension

The suspension's density as a function of the base fluid and the dispersed NEPCM particles is written as [64]:

$$\rho_b = (1-\phi)\rho_f + \phi\rho_p \tag{6}$$

The p and f subscripts denote NEPCM particles and host fluid, respectively. The density of NEPCM particles is evaluated as follows [64,65]:

$$\rho_p = \frac{(1+\imath)\rho_{co}\rho_{sh}}{\rho_{sh} + \imath\rho_{co}} \tag{7}$$

ρ_s and ρ_c are respectively the densities of the shell and core of NEPCM particles. $\imath$ is the core-shell weight ratio and is about $\imath \sim 0.447$ [35]. In addition, the density of the core is an average of the liquid and solid phases of phase change substance. The suspension's specific heat capacity is expressed as [66]:

$$C_{p,b} = \left[(1-\phi)\rho_f C_{p,f} + \phi\rho_p C_{p,p}\right]/\rho_b \tag{8}$$

Since the core of the nanoparticle undergoes a phase change, the latent heat of the phase change is involved in the specific heat capacity of the nanoparticles. The latent heat can be modeled by employing rectangular, triangle or sinusoidal profiles as follows [55,58]:

$$C_{p,p} = C_{p,co} + \frac{h_{sf}(T - T_0)}{T_{Mr}} \tag{9a}$$

$$C_{p,p} = C_{p,co} + \left\{\frac{\pi}{2}\cdot\left(\frac{h_{sf}}{T_{Mr}} - C_{p,co}\right)\cdot\sin\left(\pi\frac{T-T_0}{T_{Mr}}\right)\right\} \tag{9b}$$

$$C_{p,p} = C_{p,co} + 2\left(\frac{h_{fs}}{T_{Mr}^2} - \frac{C_{p,co}}{T_{Mr}}\right)(T - T_0) \tag{9c}$$

T_{Mr} is the temperature interval. In fact, this interval avoids the discontinuity in energy balance. The total specific heat-capacity of the nanoparticles core, involving the sensible and latent heats, are defined based on T_{Mr} [55]:

$$\begin{aligned} C_{p,p} &= C_{p,co} + \left\{\tfrac{\pi}{2}\cdot\left(\tfrac{h_{sf}}{T_{Mr}} - C_{p,co}\right)\cdot\sin\left(\pi\tfrac{T-T_0}{T_{Mr}}\right)\right\}\sigma \\ \sigma &= \begin{cases} 0 & T < T_0 \\ 1 & T_0 < T < T_1 \\ 0 & T > T_1 \end{cases} \quad \text{where}: \begin{cases} T_0 = T_{fu} - T_{Mr}/2 \\ T_1 = T_{fu} + T_{Mr}/2 \end{cases} \end{aligned} \tag{10}$$

The coefficient of the volumetric thermal volume expansion of the NEPCM-suspension is written as [66]:

$$\beta_b = (1-\phi)\beta_f + \phi\beta_p \tag{11}$$

The following linear relations are selected to relate the volume fraction of the nanoparticles to the dynamic viscosity and the thermal conductivity of a nano-particulate suspension [44,67]:

$$\frac{\mu_b}{\mu_f} = 1 + Nv\phi \tag{12b}$$

$$\frac{k_b}{k_f} = 1 + Nc\phi \tag{12a}$$

Nc and Nv of the above relations respectively denote the numbers of thermal conductivity and dynamic viscosity. It should be noted that the relations of Eqs. (12) are only valid in the case of diluted nanofluids with $\phi \leq 0.5\%$.

2.4. Dimensionless form of the governing equations

In order to generalize the model, the non-dimensionalization of the conservation equations along with the boundary and interface conditions is performed by employing the ensuing parameters:

$$\begin{aligned} X = \frac{x}{H},\ Y = \frac{y}{H},\ U = \frac{uH}{\alpha_f},\ V = \frac{vH}{\alpha_f},\ P = \frac{pH^2}{\rho_f\alpha_f^2},\ \theta \\ = \frac{T - T_c}{T_h - T_c},\ \tau = \frac{\alpha_f t}{H^2},\ A = \frac{a}{T_h - T_c} \end{aligned} \tag{13}$$

Hence, we then have:

$$\frac{\partial U}{\partial X} + \frac{\partial V}{\partial Y} = 0 \tag{14}$$

$$\varepsilon^{-2}\rho_r\left(\varepsilon\frac{\partial U}{\partial\tau} + U\frac{\partial U}{\partial X} + V\frac{\partial U}{\partial Y}\right) = -\frac{\partial P}{\partial X} + Pr\varepsilon^{-1}\mu_r\left(\frac{\partial^2 U}{\partial X^2} + \frac{\partial^2 U}{\partial Y^2}\right) - \frac{Pr}{Da}\mu_r u \tag{15}$$

$$\begin{aligned} \varepsilon^{-2}\rho_r\left(\varepsilon\tfrac{\partial V}{\partial\tau} + U\tfrac{\partial V}{\partial X} + V\tfrac{\partial V}{\partial Y}\right) &= -\tfrac{\partial P}{\partial Y} + Pr\varepsilon^{-1}\mu_r\left(\tfrac{\partial^2 V}{\partial X^2} + \tfrac{\partial^2 V}{\partial Y^2}\right) \\ &+ Ra\cdot Pr\beta_r\rho_r\theta - \tfrac{Pr}{Da}\mu_r v \end{aligned} \tag{16}$$

The non-dimensional parameters appeared in the above-written equations are:

$$\begin{aligned} Ra = \tfrac{g\rho_f\beta_f\Delta TH^3}{\alpha_f\mu_f},\ Pr = \tfrac{\mu_f}{\rho_f\alpha_f},\ Da = \tfrac{K}{H^2},\ \mu_r = 1 + Nv\phi \\ \rho_r = \left(\tfrac{\rho_b}{\rho_f}\right) = (1-\phi) + \phi\left(\tfrac{\rho_p}{\rho_f}\right),\ \beta_r = \left(\tfrac{\beta_b}{\beta_f}\right) = (1-\phi) + \phi\left(\tfrac{\beta_p}{\beta_f}\right) \end{aligned} \tag{17}$$

The thermal expansion behavior of the NEPCM particles and the base fluid is considerd similar, and, therefore, $\beta_r \sim 1$.

$$(\rho C_p)_{m,\,r}\frac{\partial\theta}{\partial\tau} + Cr\left(U\frac{\partial\theta}{\partial X} + V\frac{\partial\theta}{\partial Y}\right) = k_{m,\,r}\left(\frac{\partial^2\theta}{\partial X^2} + \frac{\partial^2\theta}{\partial Y^2}\right) \tag{18}$$

where

$$(\rho C_p)_{m,\,r} = \frac{(\rho C_p)_{m,\,b}}{(\rho C_p)_f} = \left[(1-\varepsilon)\frac{(\rho C_p)_s}{(\rho C_p)_f} + \varepsilon Cr\right] \tag{19a}$$

$$Cr=\frac{(\rho C_p)_b}{(\rho C_p)_f}=(1-\phi)+\phi\lambda+\frac{\phi}{\delta\, Ste}f \tag{19b}$$

$$k_{m,r}=\frac{k_{m,b}}{k_f}=(1-\varepsilon)\frac{k_s}{k_f}+\varepsilon(1+Nc\phi) \tag{19c}$$

where Cr is the ratio of the suspension heat capacity to the base fluid sensible heat capacity. As noticed before, the heat capacity of the suspension involves of two parts: the latent heat and the sensible heat. Moreover, the ratio of the sensible-heat capacity (λ), the range of the non-dimensional melting temperature (δ), and the Stephan number (Ste) are introduced as follows:

$$\lambda=\frac{(C_{p,co}+\imath C_{p,sh})\rho_{co}\rho_{sh}}{(\rho C_p)_f(\rho_{sh}+\imath\rho_{co})},\ \delta=\frac{T_{Mr}}{T_h-T_c},$$
$$Ste=\frac{(\rho C_p)_f(T_h-T_c)(\rho_{sh}+\imath\rho_{co})}{\alpha_f\left(h_{sf}\rho_{co}\rho_{sh}\right)} \tag{20}$$

In addition, the dimensionless fusion function, f, is defined as:

$$f=\tfrac{\pi}{2}\sin\left(\tfrac{\pi}{\delta}\left(\theta-\theta_{fu}+\delta/2\right)\right)\Xi$$
$$\Xi=\begin{cases}0 & \theta<\theta_{fu}-\delta/2\\ 1 & \theta_{fu}-\delta/2<\theta<\theta_{fu}+\delta/2\\ 0 & \theta>\theta_{fu}+\delta/2\end{cases} \tag{21}$$

Here, θ_f is the non-dimensional fusion temperature.

$$\theta_{fu}=\frac{T_{fu}-T_c}{T_h-T_c} \tag{22}$$

The non-dimensional forms of the boundary conditions can be expressed as follows:

$$X=0,\ 0\leqslant Y\leqslant 1\ :\ \ U=V=0,\ \theta=1+A\sin(\Omega\tau) \tag{23a}$$

$$X=1,\ 0\leqslant Y\leqslant 1\ :\ \ U=V=0,\ \theta=0 \tag{23b}$$

$$\begin{aligned}&Y=1,\ 0\leqslant X\leqslant 1\ :\ \ U=V=0,\ \tfrac{\partial\theta}{\partial Y}=0\\ &Y=0,\ 0\leqslant X\leqslant 1\ :\ \ U=V=0,\ \tfrac{\partial\theta}{\partial Y}=0\end{aligned} \tag{23c}$$

In Eq. (23a), the dimensionless temperature frequency is $\Omega=\omega H^2/\alpha_f$.

2.5. Heat transfer rate

The local heat transfer at the hot wall is calculated using the energy balance and non-dimensional variables as follow:

$$Nu_{Y,\tau}=-\left[(1-\varepsilon)\frac{k_s}{k_f}+\varepsilon(1+Nc\phi)\right]\left(\frac{\partial\theta}{\partial X}\right)_{Y=0} \tag{24}$$

Integrating the above-mentioned relation along the hot wall, the total rate of heat transfer at a specific time τ can be given as follows:

$$Nu_{a,\tau}=-\left[(1-\varepsilon)\frac{k_s}{k_f}+\varepsilon(1+Nc\phi)\right]\int_0^1\left(\frac{\partial\theta}{\partial X}\right)_{Y=0}dY \tag{25}$$

The average value of the Nusselt number over a period τ_p ($\tau_p=2\pi/\Omega$) is defined as:

$$Nu_a=\left(\frac{1}{\tau_p}\right)\int_{n\tau_p}^{(n+1)\tau_p}\int_0^1\left(Nu_{a,\tau}\right)dYd\tau \tag{26}$$

In order to study the effect of the nano-encapsulated particles, the following averaged Nusselt number (normalized to the averaged Nusselt number of a pure fluid) can be calculated:

$$Nu_r=\frac{Nu_a|_\varphi}{Nu_a|_{\varphi=0}} \tag{27}$$

$Nu_a|_{\varphi=0}$ is the time-averaged Nusselt number associated with the host fluid. Nu_r evaluates the impact of the presence of the NEPCM particles on the heat transfer rate compared with the host fluid. Also, streamlines which can be a good way to visualize the suspension flow is achieved by solving the following Poisson equation:

$$\frac{\partial^2\Psi}{\partial X^2}+\frac{\partial^2\Psi}{\partial Y^2}=-\left(\frac{\partial V}{\partial X}-\frac{\partial U}{\partial Y}\right) \tag{28}$$

Since the no-slip condition is valid at the walls and the walls are impermeable, the enclosure walls are a streamline with the value of zero as the boundary condition.

3. The numerical method, grid test, and validation

3.1. Numerical method

The PCM core undergoes phase change in a small band temperature. At the onset of phase change, a sharp change in the heat capacity ratio occurs, which notably changes the behavior of heat equation and increases the nonlinearity of the governing equations. The governing equations of (14)–(16) and (18), along with the boundary conditions of Eqs. (23) are solved using the finite element method. Following the finite element method, the governing equations are written in the weak form, and the following basis set $\{\gamma_k\}_{k=1}^N$ is employed to expand the x-velocity, y-velocity, the pressure equation as well as the temperature:

$$\begin{aligned}U&\approx\sum_{m=1}^N U_m\gamma_m(X,\ Y),V\approx\sum_{m=1}^N V_m\gamma_m(X,\ Y),\ P\\ &\approx\sum_{m=1}^N P_m\gamma_m(X,\ Y),\theta\approx\sum_{m=1}^N\theta_m\gamma_m(X,\ Y)\end{aligned} \tag{29}$$

The temperature and pressure equations are discretized by using linear shape functions by a similar set of the basis functions, γ. By employing the Galerkin approach, the residual equations for the velocities, pressure, and temperature at each element are obtained as:

$$\begin{aligned}R_i^1\approx{}&\frac{\rho_r}{\varepsilon}\sum_{m=1}^N U_m\int\frac{\partial\gamma_m}{\partial\tau}\gamma_i dXdY+\frac{\rho_r}{\varepsilon^2}\sum_{m=1}^N U_m\\ &\times\int\left[\left(\sum_{m=1}^N U_m\gamma_m\right)\frac{\partial\gamma_m}{\partial X}+\left(\sum_{m=1}^N V_m\gamma_m\right)\frac{\partial\gamma_m}{\partial Y}\right]\gamma_i dXdY\\ &-\sum_{m=1}^N\int\left(\sum_{m=1}^N P_m\gamma_m\right)\frac{\partial\gamma_m}{\partial X}\gamma_i dXdY+\mu_r\frac{Pr}{\varepsilon}\sum_{m=1}^N U_m\int\left[\frac{\partial\gamma_m}{\partial Y}\frac{\partial\gamma_i}{\partial Y}\right]dXdY\\ &+\mu_r\frac{Pr}{\varepsilon}\sum_{m=1}^N V_m\int\frac{\partial\gamma_m}{\partial X}\frac{\partial\gamma_i}{\partial Y}dXdY-\mu_r\frac{Pr}{Da}\int\left(\sum_{m=1}^N U_m\gamma_m\right)\gamma_i dXdY\end{aligned} \tag{30a}$$

$$\begin{aligned}R_i^2\approx{}&\frac{\rho_r}{\varepsilon}\sum_{m=1}^N V_m\int\frac{\partial\gamma_m}{\partial\tau}\gamma_i dXdY+\frac{\rho_r}{\varepsilon^2}\sum_{m=1}^N V_m\\ &\times\int\left[\left(\sum_{m=1}^N U_m\gamma_m\right)\frac{\partial\gamma_m}{\partial X}+\left(\sum_{m=1}^N V_m\gamma_m\right)\frac{\partial\gamma_m}{\partial Y}\right]\gamma_i dXdY\\ &-\sum_{m=1}^N\int\left(\sum_{m=1}^N P_m\gamma_m\right)\frac{\partial\gamma_i}{\partial Y}dXdY+\mu_r\frac{Pr}{\varepsilon}\sum_{m=1}^N U_m\int\left[\frac{\partial\gamma_m}{\partial Y}\frac{\partial\gamma_i}{\partial X}\right]dXdY\\ &+\mu_r\frac{Pr}{\varepsilon}\sum_{m=1}^N V_m\int\frac{\partial\gamma_m}{\partial X}\frac{\partial\gamma_m}{\partial X}dXdY-\mu_r\frac{Pr}{Da}\int\left(\sum_{m=1}^N V_m\gamma_m\right)\gamma_i dXdY\\ &+\beta_r\rho_r PrRa\int\left(\sum_{m=1}^N\theta_m\gamma_m\right)\gamma_i dXdY\end{aligned} \tag{30b}$$

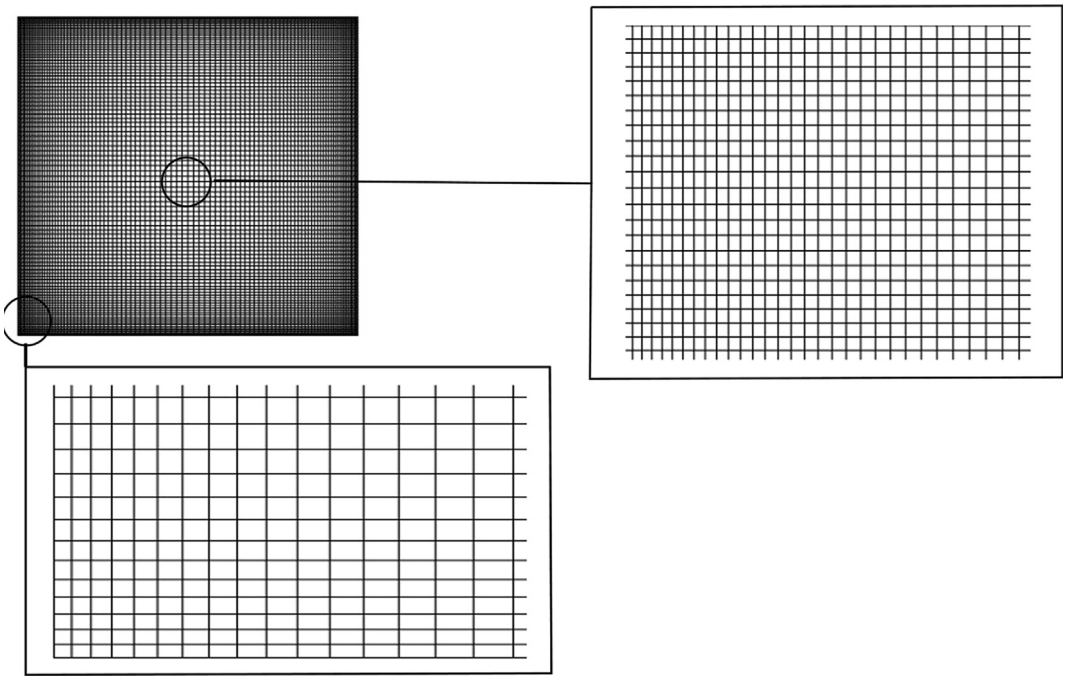

Fig. 2. The utilized grid with a size of 100 × 100.

$$R_i^3 \approx \sum_{m=1}^{N} U_m \int \frac{\partial \gamma_m}{\partial X}\gamma_i dXdY + \sum_{m=1}^{N} V_m \int \frac{\partial \gamma_m}{\partial Y}\gamma_i dXdY \tag{30c}$$

$$\begin{aligned} R_i^4 \approx {} & (\rho C_p)_{m,r} \sum_{m=1}^{N} \theta_m \int \frac{\partial \gamma_m}{\partial \tau}\gamma_i dXdY \\ & + Cr \sum_{m=1}^{N} \theta_m \int \left[\left(\sum_{m=1}^{N} U_m \gamma_m \right) \frac{\partial \gamma_m}{\partial X} + \left(\sum_{m=1}^{N} V_m \gamma_m \right) \frac{\partial \gamma_m}{\partial Y} \right] \gamma_m dXdY \\ & + k_{m,r} \sum_{m=1}^{N} \theta_k \int \left[\frac{\partial \gamma_m}{\partial X}\frac{\partial \gamma_i}{\partial X} + \frac{\partial \gamma_m}{\partial Y}\frac{\partial \gamma_i}{\partial Y} \right] dXdY \end{aligned} \tag{30d}$$

The integrals in the residual equations are numerically integrated using Gaussian quadrature with second-order accuracy. Due to sharp grow of heat capacity ratio at the onset of the phase change of NEPCMs particles, using an adequate time step is essential. The selection of time step is controlled automatically using a Backward Differentiation Formula (BDF) with a free time-step scheme, within a free time-step selection in an order between one and two [68]. The residual equations are iteratively solved by Newton method employing a PARDISO solver [69–71]. The iterations with a Newtonian damping factor of 0.8 are repeated until with a residual error of O (10^{-6}) is achieved. The streamline equation is solved independently by using the obtained velocity field.

3.2. Grid check

The discretization of the computational domain is performed into a regular mesh consisting of $N \times N$ rectangular elements. The mesh was stretched with the stretching ratio of 10 near the walls to adequately capture the temperature gradients, and the mesh is progressively coarsened towards the center of the cavity. A view of the mesh size of 100 × 100 is depicted in Fig. 2. Different grid sizes are investigated to adopt a grid with adequate accuracy and low computational cost. For this reason, the average value of Nusselt number at the hot wall and the magnitude of stream function $|\Psi|_{max}$ over one period (time between τ_p and $2\tau_p$) in the whole surface of the cavity are selected as criteria to determine the sufficiently fine mesh. According to Table 2, the grid size of 100 × 100 represents the number of elements above which the obtained values of averaged-time Nusselt number and $|\Psi|_{max}$ show a negligible difference compared to grids with finer meshes. Therefore, the grid size of 100 × 100 presents very good precision and is adopted for the numerical study.

3.3. Validation

The results of the present study are evaluated through several published works to validate the correctness of the utilized code. At the first comparison, the work of Kahveci [72] re-simulated. Kahveci [72] studied the natural convection heat transfer of a sus-

Table 2
Grid check results for Nu_a and $|\Psi|_{max.}$

Case number (i)	Grid size	Nu_a	Δ_1	$\lvert\Psi\rvert_{max}$	Δ_2
1	25 × 25	25.02	0.0823	25.196	0.03421
2	50 × 50	25.73	0.0524	25.421	0.02506
3	75 × 75	26.95	0.0048	25.845	0.00824
4	100 × 100	27.08	–	26.058	–
5	125 × 125	27.08	0.0000	26.080	0.00084
6	150 × 150	27.09	0.0003	26.100	0.00160

$\Delta_1 = \frac{|Nu_{i+1} - Nu_i|}{Nu_i} \times 100$, $\Delta_2 = \frac{|\psi_{i+1} - \psi_i|}{\psi_i} \times 100$.

pension of water and the Al_2O_3 nanoparticles filling a square enclosure. The left and right bounds of the studied square domain were kept at the higher and lower temperatures of T_h and T_c, respectively. While the horizontal bounds were adiabatic. The average Nusselt number acquired in the present code, and the work of Kahveci [72] are tabulated in Table 3. The outcomes of the current solution are further verified by comparing the heat transfer rates obtained from the applied code in this paper with the heat transfer rates presented by Nithiarasu et al. [73]. This verification is performed to approve the correct implementation of the governing equations in the employed code for a porous medium. The high and low temperatures were imposed on the left and right vertical walls and the other walls were adiabatically isolated. The results are tabulated in Table 4 for the difference values of governing parameters and Pr = 1.

As a transient natural convection flow, an evaluation is conducted using the numerical results of Kalabin et al. [74]. The geometry studied by Kalabin et al. [74] was a square cavity with sinusoidally varying time-periodic temperature imposed on its left wall. The opposite bound was isothermally kept at the low temperature. As depicted in Fig. 3, the average Nusselt number of the present investigation is compared to the one reported in [74] for $Ra = 2 \times 10^5$, Pr = 1, and $\Omega = 20\pi$. As shown in Fig. 3, a good agreement is obtained in the results of the present study compared to those of Kalabin et al. [74].

Table 3
The average Nusselt numbers of the present investigation and Kahveci [72] for $Ra = 10^6$.

	ϕ = 0.1	ϕ = 0.05	ϕ = 0
Current work	10.3	9.76	9.20
Kahveci	10.297	9.783	9.23

Table 4
The average Nusselt number computed in the current work and that of [73]

Da	Ra	ε	Present study	Reference [73]
10^{-6}	10^7	0.4	1.078	1.078
10^{-4}	10^7	0.9	9.322	9.202
10^{-2}	10^4	0.4	1.360	1.408
10^{-2}	10^5	0.9	3.92	3.91

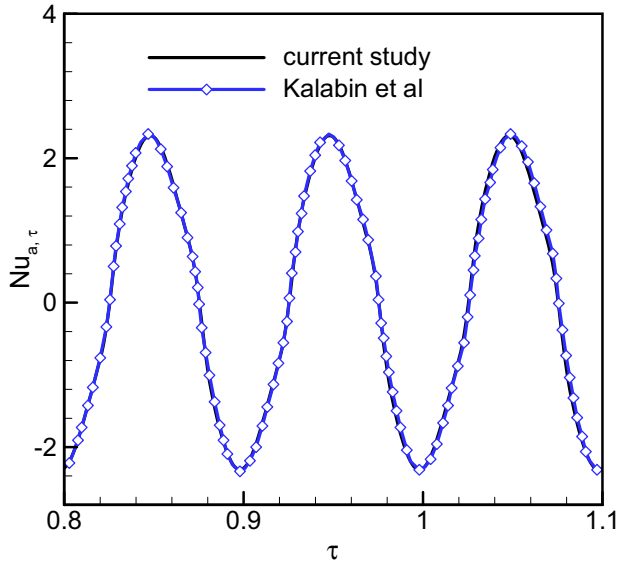

Fig. 3. The time history of the Nusselt number obtained by Kalabin et al. [74] and the outcomes of the current work.

4. Results and discussions

The effect of a parameter is assessed by varying its value in a limited range and examining the results accordingly. A certain range of parameters was used to study the change of the qualitative behavior of the suspension of NEPCM particles and water. The values of ratio of the heat capacity of the NEPCM particles to the base fluid (λ), dynamic viscosity (Nv), and thermal conductivity (Nc) numbers are adopted following the experiments of Barlak et al. [35]. Also, as mentioned in the text, the relations of thermal conductivity and dynamic viscosity are applicable for a low concentration of particles $\phi \leq 0.5\%$. The porosity and Darcy number describe the characteristics of the porous medium that can be included a wide range of values. In fact, considering the porosity definition, the selected values for porosity is entirely desirable. Besides, regarding the characterization length, the selected values for the Darcy number can be developed for practical application.

Moreover, as pointed out in the text, the fusion temperature is non-dimensionalized based on the temperature difference of the hot and cold walls. Hence, the dimensionless values of it, i.e., θ_{fu}, can be varied from zero to 1. In the end, the selected values for the melting range and Stefan number for the organic PCM forming the core of MEPCM particles are practical.

The ranges of the alterable parameters are: Rayleigh number $10^5 \leq Ra \leq 10^7$, dimensionless fusion temperature $0.05 \leq \theta_{fu} \leq 1$, porosity $0.3 \leq \varepsilon \leq 0.9$, Darcy number $10^{-5} \leq Da \leq 10^{-1}$, non-dimensional frequency $0.01\pi \leq \Omega \leq \pi$, dimensionless amplitude $0.0 \leq A \leq 1$ and the NEPCM volume fraction $0.0 \leq \phi \leq 5\%$. The default value of non-dimensional parameters is adopted as Nc = 23.8, Nv = 12.5, λ = 0.32, Pr = 6.2, Ste = 0.2, δ = 0.05, θ_{fu} = 0.1, $Ra = 10^7$, Da = 0.1, ϕ = 0.05, $\Omega = \pi$, A = 1, and ε = 0.8. These parameters represent the default values that will be used throughout the study other indicated otherwise. To emphasize the effect of a defined parameter on the results, it will be varied in a selected interval and the results will be reported accordingly.

The variation of the time history of Nusselt number of the hot wall $Nu_{a,\tau}$ is depicted in Fig. 4(a). It is clear that $Nu_{a,\tau}$ shows a periodic variation accordingly with the temperature variation of the hot wall, so that $Nu_{a,\tau}$ reaches to maximum and minimum values when the hot wall temperature is maximum (at $0.25\tau_p$, $1.25\tau_p$, $2.25\tau_p$, and $3.25\tau_p$) and minimum (at $0.75\tau_p$, $1.75\tau_p$, $2.75\tau_p$, and $3.75\tau_p$) respectively. Indeed, when the temperature of the hot wall is at its highest, the heat transfer in the enclosure reaches its peak due to the increased temperature difference between the hot and cold walls. It should be noted that based on the selected default values for the hot wall temperature ($\theta_h = 1$ and $A = 1$), the minimal value of the hot wall temperature is equal to the cold wall temperature. So when the hot wall temperature is minimum, no heat transfer is occurring in the cavity and $Nu_{a,\tau} = 0$. Overall, the heat transfer inside the enclosure is varying periodically with intervals of very active heat transfer followed by intervals with zero heat transfer. Moreover, $Nu_{a,\tau}$ is oscillating around a mean value Nu_a, which corresponds to the value that would have been obtained if the hot wall temperature was steady ($A = 0$).

The effect of the presence of the NEPCM particles in the fluid on the heat transfer characteristics can be analyzed by looking at the variation of Nu_r as a function of the NEPCM volume fraction ϕ as shown in Fig. 4(b). Raising ϕ obviously tends to enhance heat transfer by increasing the value of Nu_r. The maximum value of Nu_r is reached for $\phi = 0.05$. As the NEPCM suspension is assumed to be diluted, it can be deduced that the optimal value of ϕ is 5%.

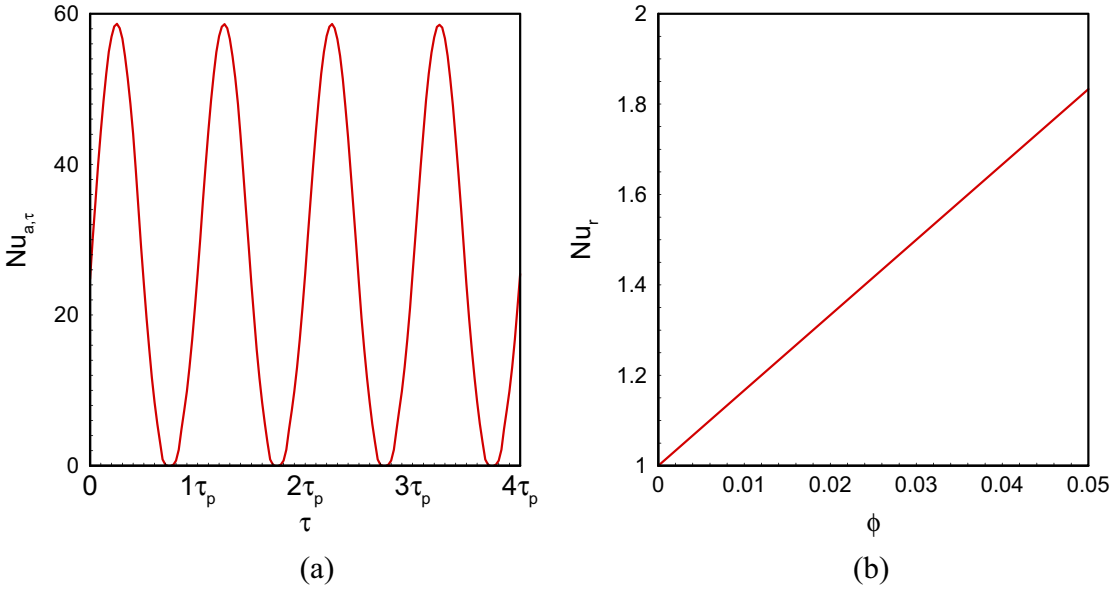

Fig. 4. The Nusselt number; (a) time history of $Nu_{a,\tau}$, and (b): Nu_r as a function of NEPCM volume fraction.

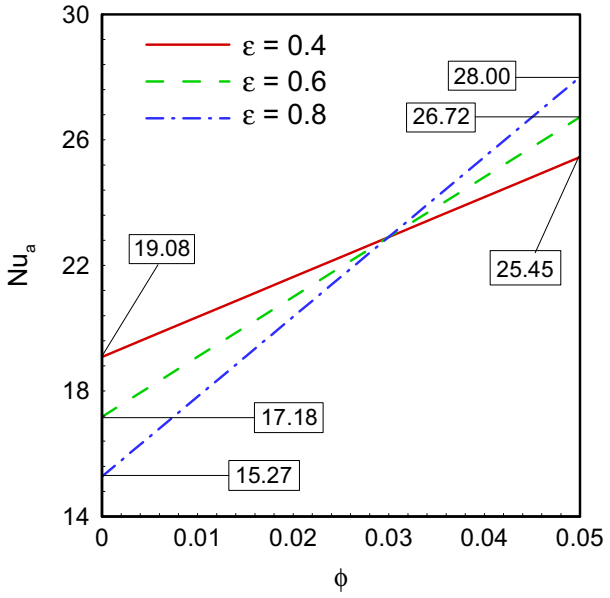

Fig. 5. The variation of the time-averaged Nusselt number for various values of ϕ and porosity.

An increase of 80% in the value of Nu_a is achieved when using a suspension with $\phi = 5\%$ compared to the case with pure fluid.

Fig. 5 illustrates the variation of time-averaged Nusselt number of the hot wall over one period Nu_a as a function of NEPCM particles, for different values of the porosity ε. For low values of ϕ, rising the porosity ε decreases the value ofNu_a. When ϕ is increased, typically above 3%, Nu_a starts increasing with the rise of ε. This suggests that the porosity greatly affects the impact of the NEPCM particles on the heat transfer. While a high porosity tends to enhance heat transfer in a cavity with NEPCM suspension with a higher volume fraction ϕ, its effect is less advantageous when ϕ is decreased. Indeed, when the porosity is reduced, the volume of the solid matrix increases. Hence, due to the weak thermal conductivity of glass balls, melting of the PCM cores is slowed down and the NEPCM particles contribution of the to the overall heat transfer is diminished, and, thus, a reduced porosity with a lower NEPCM fraction presents a better heat transfer performance and leads to a higher value of Nu_a. An optimal heat transfer is therefore obtained for $\phi = 5\%$ and $\varepsilon = 0.4$.

The effect of Rayleigh number Ra on the variation of $Nu_{a,\tau}$ as a function of time is shown in Fig. 6. It is clear that the amplitude of $Nu_{a,\tau}$ increases with the rise of Ra. A significant increase in the amplitude is shown when Ra is increased from 10^5 to 10^7. In fact, Ra represents the relative importance of the natural convection driving forces in the cavity. An increase of Ra indicated that buoyancy forces dominate the viscous resistive forces and, consequently, stronger convection occurs, leading to a higher amplitude of $Nu_{a,\tau}$.

To better illustrate the effects of Ra and ε on the heat transfer in the enclosure, the variation of Nu_a as a function of Ra for various values of ε is shown in Fig. 7. Increasing ε inhibits heat transfer

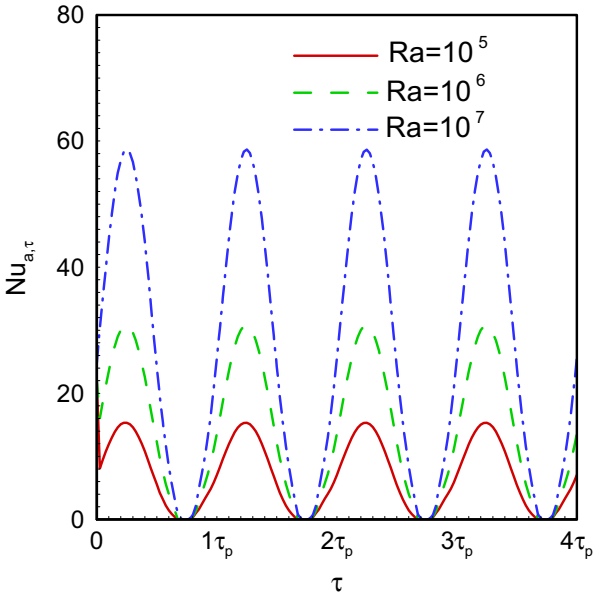

Fig. 6. The time history of Nusselt number $Nu_{a,\tau}$ for three various values of Ra number.

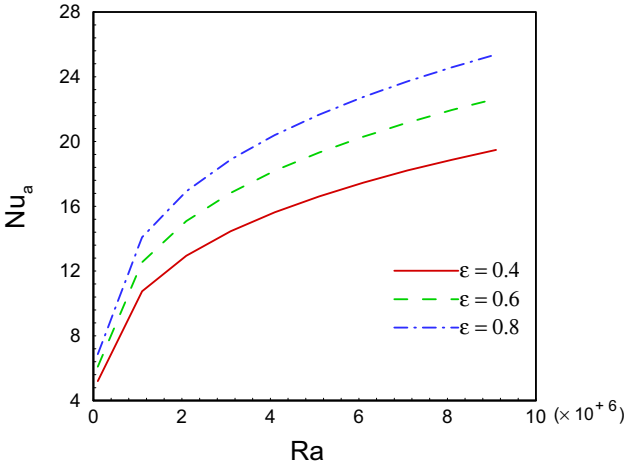

Fig. 7. The time-averaged Nusselt number aginst various values of *Ra* number for various values of porosity.

in the enclosure for all the values of *Ra*. Similarly, the effect of *Ra* on Nu_a is independent of ε. The effects of the medium porosity and *Ra* on heat transfer in the enclosure are thus independent of each other.

The isotherm contours and the flow streamlines at different instants are shown in Fig. 8. At $\tau = \tau_p$ (Fig. 8(a), the hot wall temperature is $\theta = 1$, and a temperature gradient is present in the cavity. The isotherms $\theta = 0.2$ to $\theta = 0.8$ start near the hot wall then continue horizontally until the cold wall. The isotherm $\theta = 0.1$ starts from the middle of the bottom wall until the hot wall, while the isotherm $\theta = 0.9$ finishes very close to the hot wall. The streamlines show a flow covering the enclosure, with a zone with higher velocity near the hot wall. At $\tau = 0.25\tau_p$, the temperature of the hot wall is $\theta = 2$ which gives rise to a greater temperature gradient in the enclosure.

The streamlines present a symmetrical behavior with zones of high velocity near the hot and cold walls. The isotherm contours from 0 to 0.9 are limited in the bottom half of the cavity, while isotherms with higher temperature values occupy the importance. This observation indicates that the position of the zone of phase change of the PCM cores, which falls near the isotherm with a temperature equal to θ_{fu}, goes down in the cavity when τ increases from τ_p to $1.25\tau_p$. At $\tau = 1.5\tau_p$ (Fig. 8(c)), the the hot wall temperature drops back to $\theta = 1$, and the isotherm contours are very similar to the ones obtained for $\tau = \tau_p$. Flow with higher velocity is present near the cold wall. Finally, Fig. 8(d) shows that when the hot wall temperature is 0, i.e., equal to that of the cold wall, the flow is very slow, and there is no temperature gradient in the cavity. Overall, the distribution of the isotherms and the streamlines

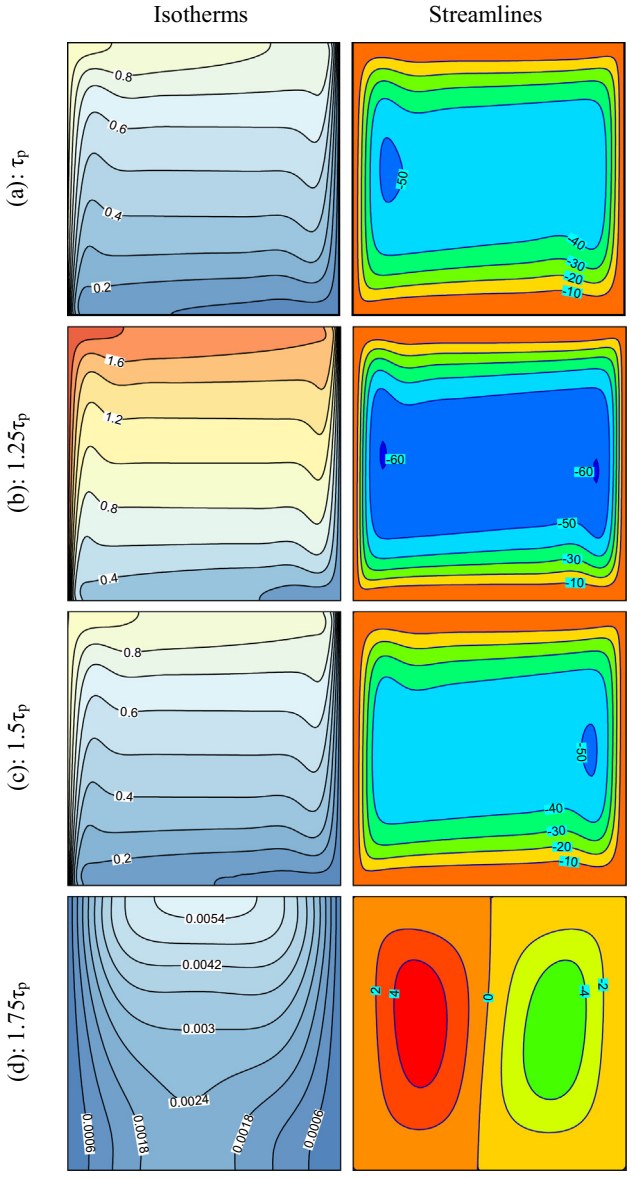

Fig. 8. The isotherms and streamlines during time.

inside the enclosure changes significantly with time due to the periodic variation of the hot wall temperature.

The contours of the heat capacity ratio *Cr* contours for different values of the fusion temperature θ_{fu} at $\tau = \tau_p$ are displayed in Fig. 9. The dark red ribbons correspond to the zones in which the

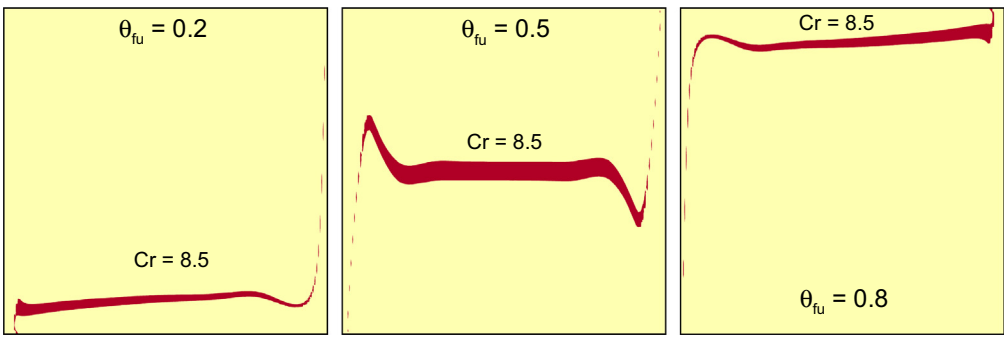

Fig. 9. The heat capacity ratio contours at different values of dimensionless fusion temperature at τ_p.

phase change of the NEPCM is occurring. It is clear that increasing θ_{fu} tends to push the phase change towards the top wall.

In fact, as mentioned earlier, the PCM undergoes phase change when the nearby temperature is close to its fusion temperature θ_{fu}. As discussed in Fig. 8, the isotherms with higher temperature are above those with lower temperature. Therefore, when θ_{fu} is increased, the position of the isotherm corresponding to its value will be higher and closer to the top wall in the enclosure, which explains the shift of the phase change zone towards the top wall.

Fig. 10 depicts the variation of $Nu_{a,\tau}$as a function of θ_{fu} at two distinct instants, $\tau = \tau_p$ and $\tau = 1.25\tau_p$ for different values of Darcy number *Da*. It is obvious that increasing *Da* improves heat transfer inside the cavity for all the values of θ_{fu}. In fact, a higher value of *Da* signals an increase of the porous medium permeability. The suspension is, therefore, flowing in the cavity with more ease and convective heat transfer is enhanced. It is also shown that at $\tau = \tau_p$, i.e. when the hot wall temperature amplitude is 0 and the value of $Nu_{a,\tau}$ is the average value Nu_a. $Nu_{a,\tau}$ presents a maximum when θ_{fu} is in the interval [0.25; 0.75]. Similarly, at $\tau = 1.25\tau_p$, i.e. when the hot wall is at its maximum temperature $\theta = 2$, the effect of $Nu_{a,\tau}$ remains increasing with θ_{fu} when θ_{fu} is between 0.5 and 1. Fig. 10 thus shows that heat transfer is thus enhanced when the PCM fusion temperature is far from the temperatures of the hot and cold walls. An optimal heat transfer is achieved when θ_{fu} is in the range $[0.25\theta_h; 0.75\theta_h]$.

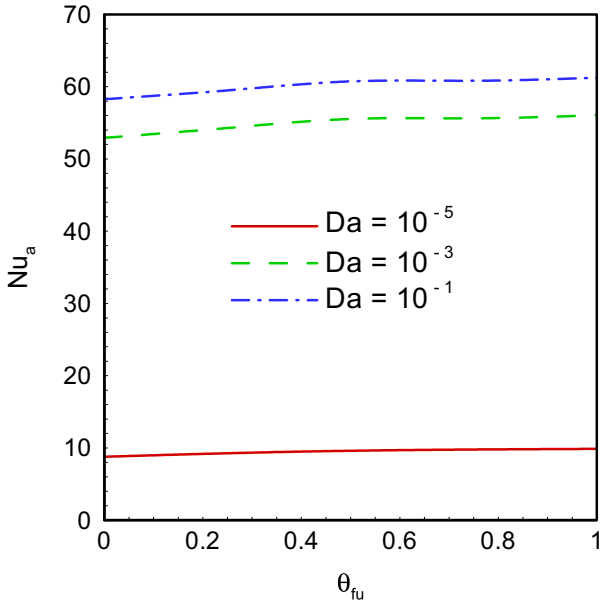

Fig. 10. The variation of time-averaged Nusselt number aginst the fusion temperature (θ_{fu}) for different values of *Da*.

The effect of Darcy number *Da* on the *Cr* contours inside the cavity is depicted in Fig. 11. For $Da = 10^{-5}$ the melting is occurring over a straight line near the cold wall. When *Da* is increased the melting zone shifts towards the center in the bottom part of the cavity. This suggests that while increasing *Da* facilitates the suspension of the flow inside the medium, it has an effect on the temperature distribution in the cavity and consequently affects the zone of phase change of the PCM cores. Fig. 11 illustrates then the contribution of the NEPCM particles to the overall heat transfer in the cavity as discussed in Fig. 9.

The variation of $Nu_{a,\tau}$ during the time is shown in Fig. 12 for various values of amplitude (A) and the porosity (ε). Three different values of the temperature frequency Ω are It is shown that the frequency of $Nu_{a,\tau}$ is equal to that of the temperature (Ω) and that the average value of $Nu_{a,\tau}$ remains the same even when Ω is varied. Comparing Fig. 12(a) to (b) shows that raising A increases the amplitude of $Nu_{a,\tau}$. Therefore, $Nu_{a,\tau}$ follows a periodic variation with a frequency equa to that of the temperature variation and with an amplitude that rises with the increase of that of the temperature. A comparison between Fig. 12(b) and (c) confirms the fact that a higher porosity increases the average value Nu_a and enhances heat transfer. However, its impact on the amplitude of $Nu_{a,\tau}$ is relatively limited.

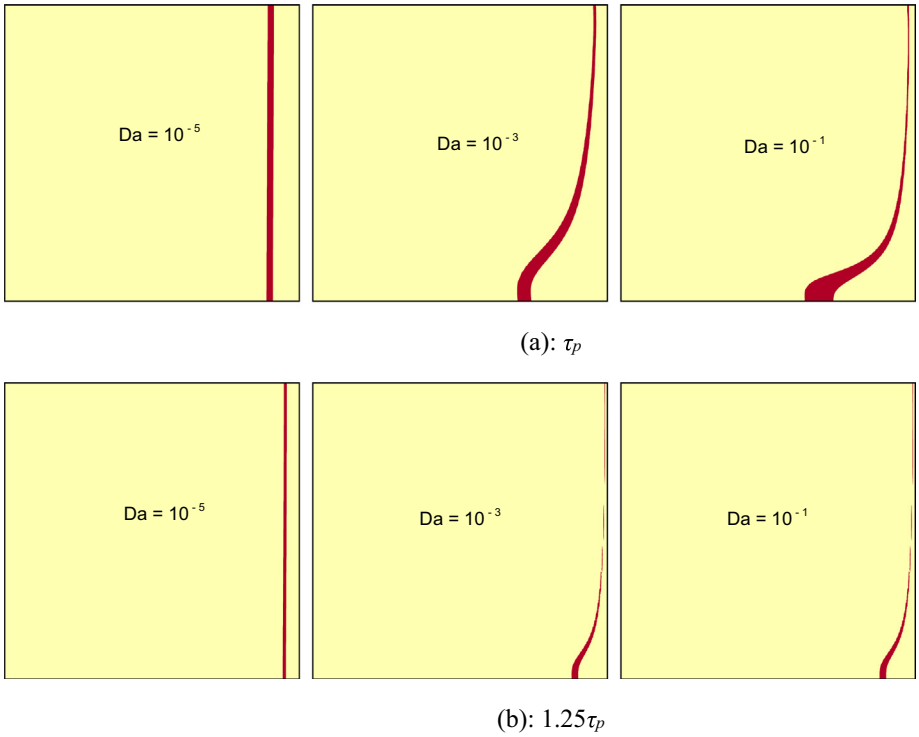

Fig. 11. The heat capacity ratio contours in different values of Darcy number in specific times.

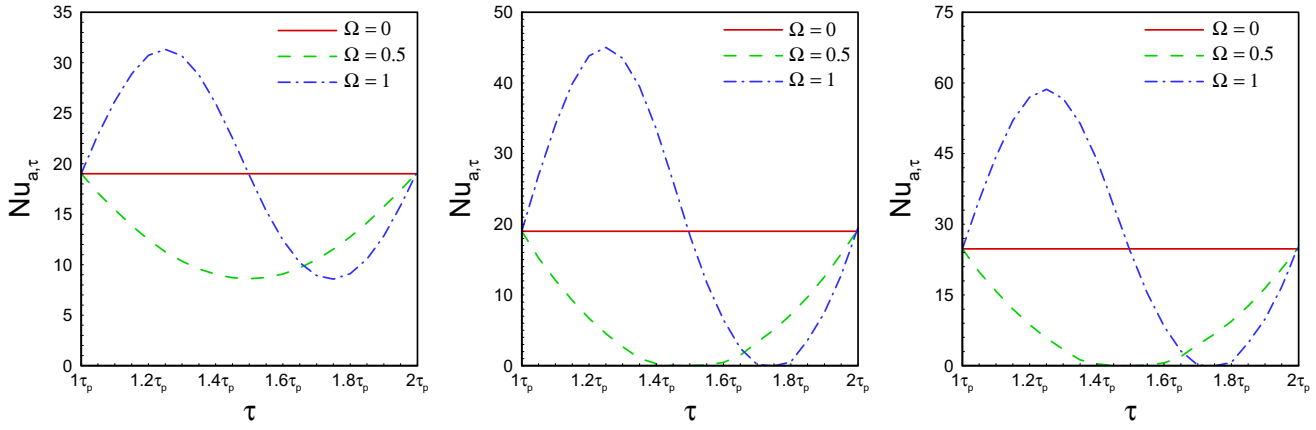

(a): $A = 0.5$, $\varepsilon = 0.4$ (b): $A = 1$, $\varepsilon = 0.4$ (c): $A = 1$, $\varepsilon = 0.8$

Fig. 12. The effect of various values of porosity and Ω on the Nusselt number ($Nu_{a,\tau}$) during time when A = 0.5 and A = 1.

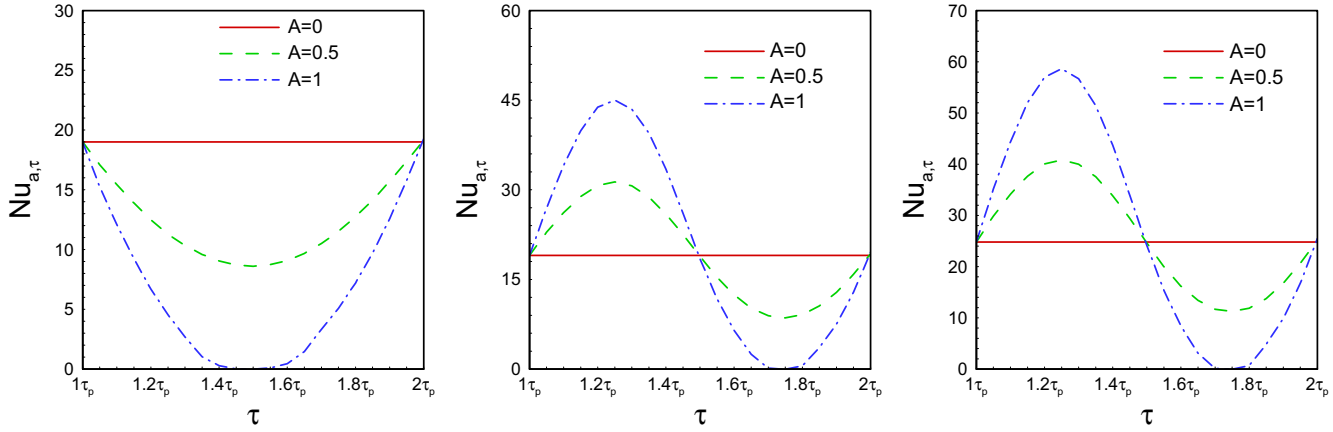

(a): $\Omega = 0.5\pi$, $\varepsilon = 0.4$ (b): $\Omega = \pi$, $\varepsilon = 0.4$ (c): $\Omega = \pi$, $\varepsilon = 0.8$

Fig. 13. The effect of various values of porosity and A on the Nusselt number ($Nu_{a,\tau}$) during time when $\Omega = 0.5\pi$ and $\Omega = \pi$.

To better illustrate the impact of amplitude, frequency, and porosity on heat transfer in the enclosure, the variation of $Nu_{a,\tau}$ as a function of time is plotted in Fig. 13 for different values of A, Ω, and ε. It is confirmed that the amplitude of $Nu_{a,\tau}$ increases when A is increased, for all the values of Ω, and ε. It is equally verified that $Nu_{a,\tau}$ frequency is always the same as Ω. Finally, comparing Fig. 13(b) to (c) confirms the improvement of heat transfer due to the increase of ε, as indicated by the increase of the average value Nu_a. It is shown that doubling the porosity (cases (b) and (c)) can increase the heat transfer by up to 33% for all the non-zero values of the temperature amplitude. To summarize, the variation of $Nu_{a,\tau}$ is periodic and presents a frequency equal to that of the hot wall temperature and an amplitude that increases accordingly with the rise of the temperature amplitude and/or the medium porosity.

5. Conclusion

The unsteady free convection heat transfer in a cavity filled with a porous medium and saturated with a suspension of NEPCM was theoretically studied. The hot wall of the cavity was subject to a periodic wall temperature while the cold wall was kept at a constant cold temperature. The hot temperature and cold temperatures were respectively at higher and lower temperatures than the fusion temperature of nanoparticles, and hence, the PCM core of nanoparticles undergoes a phase change. On phase-change, a significant amount of heat can be stored/released. The effect of the presence of the porous medium and NEPCM particles on the heat transfer behavior of the cavity is investigated in the form of isotherm contours and heat capacity contours as well as time history of Nusselt number and average Nusselt number. The results of the numerical studies can be summarized as follows:

- When the temperature of the hot wall of the cavity is varying periodically with time, $Nu_{a,\tau}$ shows a periodic variation having a frequency equal to that of the hot wall temperature and an amplitude which increases accordingly with the increase of the temperature amplitude. The heat transfer inside the enclosure is thus characterized by periods of active heat transfer followed by periods of zero heat transfer and so on. The average value Nu_a of $Nu_{a,\tau}$ remains constant even when the temperature amplitude and/or frequency are varied.
- Increasing the volume fraction ϕ of the NEPCM particles enhances heat transfer inside the cavity. Nonetheless, as the suspension is assumed to be diluted, $\phi = 5\%$ is the fraction which corresponds to an optimal heat transfer.

- Increasing the porosity enhances heat transfer when the NEPCM volume fraction ϕ is high, typically higher than 3%. When ϕ is below this value, porosity plays an opposite role, and improvement of the heat transfer performance in the cavity can be observed in a lower porosity.
- A higher value of Rayleigh number *Ra* leads to heat transfer enhancement due to the increased relative importance of buoyancy forces which dominate the viscous forces, resulting in stronger convective effects.
- Increasing the fusion temperature θ_{fu} of the NEPCM cores changes the location at which phase change is occurring, which depends on the temperature distribution inside the cavity. In addition, heat transfer is better enhanced when θ_{fu} is not close to the hot and cold wall temperatures. An optimal enhancement is achieved when θ_{fu} is between 0.25 and 0.75.
- Increasing Darcy number *Da* improves heat transfer in the cavity as it eases the flow motion of the suspension in the pores and consequently boosts the convection.

In the present study, the unsteady flow and heat transfer of NEPCMs in a square enclosure with a periodic temperature was investigated, and the effect of the fusion temperature and porosity was found to be important. The suspension of NEPCMs can be utilized as a phase change heat sink or phase change thermal energy storage. Therefore the energy storage response time and capacity of NEPCM suspensions can be subject of future studies.

References

[1] S. Mehryan, M.A. Sheremet, M. Soltani, M. Izadi, Natural convection of magnetic hybrid nanofluid inside a double-porous medium using two-equation energy model, J. Mol. Liq. 277 (2019) 959–970.
[2] I.V. Miroshnichenko, M.A. Sheremet, H.F. Oztop, N. Abu-Hamdeh, Natural convection of alumina-water nanofluid in an open cavity having multiple porous layers, Int. J. Heat Mass Transf. 125 (2018) 648–657.
[3] M.S. Astanina, M. Sheremet, C.J. Umavathi, Unsteady natural convection in a partially porous cavity having a heat-generating source using local thermal non-equilibrium model, Int. J. Numer. Meth. Heat Fluid Flow (2018).
[4] A.K. Asl, S. Hossainpour, M. Rashidi, M. Sheremet, Z. Yang, Comprehensive investigation of solid and porous fins influence on natural convection in an inclined rectangular enclosure, Int. J. Heat Mass Transf. 133 (2019) 729–744.
[5] R. Mohebbi, A.A. Delouei, A. Jamali, M. Izadi, A.A. Mohamad, Pore-scale simulation of non-Newtonian power-law fluid flow and forced convection in partially porous media: thermal lattice Boltzmann method, Phys. A: Stat. Mech. Appl. 525 (2019) 642–656.
[6] M.A. Ismael, H.S. Ghalib, Double diffusive natural convection in a partially layered cavity with inner solid conductive body, Sci. Iran 25 (2018) 2643–2659.
[7] M.A. Sheremet, I. Pop, Effect of local heater size and position on natural convection in a tilted nanofluid porous cavity using LTNE and Buongiorno's models, J. Mol. Liq. 266 (2018) 19–28.
[8] A.I. Alsabery, T. Tayebi, A.J. Chamkha, I. Hashim, Effect of rotating solid cylinder on entropy generation and convective heat transfer in a wavy porous cavity heated from below, Int. Commun. Heat Mass Transf. 95 (2018) 197–209.
[9] A. Alsabery, A. Chamkha, I. Hashim, P. Siddheshwar, Effects of nonuniform heating and wall conduction on natural convection in a square porous cavity using LTNE model, J. Heat Transf. 139 (2017) 122008.
[10] J. Merkin, I. Pop, Natural convection boundary-layer flow in a porous medium with temperature-dependent boundary conditions, Transp. Porous Media 85 (2010) 397–414.
[11] J.H. Merkin, A.M. Rohni, S. Ahmad, I. Pop, On the temperature slip boundary condition in a mixed convection boundary-layer flow in a porous medium, Transp. Porous Media 94 (2012) 133–147.
[12] Y. Lok, J. Merkin, I. Pop, Mixed convection boundary-layer flow over a vertical surface embedded in a porous material subject to a convective boundary condition, Transp. Porous Media 98 (2013) 451–463.
[13] K. Khanafer, K. Vafai, M. Lightstone, Buoyancy-driven heat transfer enhancement in a two-dimensional enclosure utilizing nanofluids, Int. J. Heat Mass Transf. 46 (2003) 3639–3653.
[14] I. Hashim, A. Alsabery, M. Sheremet, A. Chamkha, Numerical investigation of natural convection of Al2O3-water nanofluid in a wavy cavity with conductive inner block using Buongiorno's two-phase model, Adv. Powder Technol. 30 (2019) 399–414.
[15] C. Sivaraj, M. Sheremet, MHD natural convection and entropy generation of ferrofluids in a cavity with a non-uniformly heated horizontal plate, Int. J. Mech. Sci. 149 (2018) 326–337.
[16] C. Revnic, M. Ghalambaz, T. Groşan, M. Sheremet, I. Pop, Impacts of non-uniform border temperature variations on time-dependent nanofluid free convection within a trapezium: Buongiorno's nanofluid model, Energies 12 (2019) 1461.
[17] A. Dogonchi, M. Waqas, S. Seyyedi, M. Hashemi-Tilehnoee, D. Ganji, CVFEM analysis for Fe3O4–H2O nanofluid in an annulus subject to thermal radiation, Int. J. Heat Mass Transf. 132 (2019) 473–483.
[18] A.I. Alsabery, T. Armaghani, A.J. Chamkha, M.A. Sadiq, I. Hashim, Effects of two-phase nanofluid model on convection in a double lid-driven cavity in the presence of a magnetic field, Int. J. Numer. Meth. Heat Fluid Flow 29 (2019) 1272–1299.
[19] M. Ghalambaz, A. Doostani, E. Izadpanahi, A.J. Chamkha, Conjugate natural convection flow of Ag–MgO/water hybrid nanofluid in a square cavity, J. Therm. Anal. Calorim. (2019) 1–16.
[20] A. Tahmasebi, M. Mahdavi, M. Ghalambaz, Local thermal nonequilibrium conjugate natural convection heat transfer of nanofluids in a cavity partially filled with porous media using Buongiorno's model, Numer. Heat Transf. Part A: Appl. 73 (2018) 254–276.
[21] A. Chamkha, M. Ismael, A. Kasaeipoor, T. Armaghani, Entropy generation and natural convection of CuO-water nanofluid in C-shaped cavity under magnetic field, Entropy 18 (2016) 50.
[22] S.M. Seyyedi, A. Dogonchi, D. Ganji, M. Hashemi-Tilehnoee, Entropy generation in a nanofluid-filled semi-annulus cavity by considering the shape of nanoparticles, J. Therm. Anal. Calorim. (2019) 1–15.
[23] A. Dogonchi, T. Armaghani, A.J. Chamkha, D. Ganji, Natural convection analysis in a cavity with an inclined elliptical heater subject to shape factor of nanoparticles and magnetic field, Arab. J. Sci. Eng. (2019) 1–13.
[24] A. Chamkha, A. Dogonchi, D. Ganji, Magnetohydrodynamic nanofluid natural convection in a cavity under thermal radiation and shape factor of nanoparticles impacts: a numerical study using CVFEM, Appl. Sci. 8 (2018) 2396.
[25] A. Dogonchi, Heat transfer by natural convection of Fe3O4-water nanofluid in an annulus between a wavy circular cylinder and a rhombus, Int. J. Heat Mass Transf. 130 (2019) 320–332.
[26] A. Dogonchi, A.J. Chamkha, M. Hashemi-Tilehnoee, S. Seyyedi, D. Ganji, Effects of homogeneous-heterogeneous reactions and thermal radiation on magneto-hydrodynamic Cu-water nanofluid flow over an expanding flat plate with non-uniform heat source, J. Central South Univ. 26 (2019) 1161–1171.
[27] S. Sivasankaran, A. Alsabery, I. Hashim, Internal heat generation effect on transient natural convection in a nanofluid-saturated local thermal non-equilibrium porous inclined cavity, Phys. A: Stat. Mech. Appl. 509 (2018) 275–293.
[28] A.S. Dogonchi, A.J. Chamkha, S.M. Seyyedi, M. Hashemi-Tilehnoee, D.D. Ganji, Viscous dissipation impact on free convection flow of Cu-water nanofluid in a circular enclosure with porosity considering internal heat source, J. Appl. Comput. Mech. 5 (2019) 717–726.
[29] I. Pop, M. Ghalambaz, M. Sheremet, Free convection in a square porous cavity filled with a nanofluid using thermal non equilibrium and Buongiorno models, Int. J. Numer. Meth. Heat Fluid Flow 26 (2016) 671–693.
[30] A. Alsabery, A. Chamkha, H. Saleh, I. Hashim, Natural convection flow of a nanofluid in an inclined square enclosure partially filled with a porous medium, Sci. Rep. 7 (2017) 2357.
[31] A.J. Chamkha, M.A. Ismael, Natural convection in differentially heated partially porous layered cavities filled with a nanofluid, Numer. Heat Transf. Part A: Appl. 65 (2014) 1089–1113.
[32] A. Dogonchi, M. Hashemi-Tilehnoee, M. Waqas, S.M. Seyyedi, I. Animasaun, D. Ganji, The influence of different shapes of nanoparticle on Cu-H2O nanofluids in a partially heated irregular wavy enclosure, Phys. A: Stat. Mech. Appl. (2019) 123034.
[33] A. Dogonchi, M. Waqas, D. Ganji, Shape effects of Copper-Oxide (CuO) nanoparticles to determine the heat transfer filled in a partially heated rhombus enclosure: CVFEM approach, Int. Commun. Heat Mass Transf. 107 (2019) 14–23.
[34] A. Dogonchi, M. Waqas, S.M. Seyyedi, M. Hashemi-Tilehnoee, D. Ganji, Numerical simulation for thermal radiation and porous medium characteristics in flow of CuO-H2O nanofluid, J. Braz. Soc. Mech. Sci. Eng. 41 (2019) 249.
[35] S. Barlak, O.N. Sara, A. Karaipekli, S. Yapıcı, Thermal conductivity and viscosity of nanofluids having nanoencapsulated phase change material, Nanoscale Microscale Thermophys. Eng. 20 (2016) 85–96.
[36] A. Jamekhorshid, S. Sadrameli, M. Farid, A review of microencapsulation methods of phase change materials (PCMs) as a thermal energy storage (TES) medium, Renew. Sustain. Energy Rev. 31 (2014) 531–542.
[37] W. Su, J. Darkwa, G. Kokogiannakis, Review of solid–liquid phase change materials and their encapsulation technologies, Renew. Sustain. Energy Rev. 48 (2015) 373–391.
[38] G. Fang, H. Li, F. Yang, X. Liu, S. Wu, Preparation and characterization of nano-encapsulated n-tetradecane as phase change material for thermal energy storage, Chem. Eng. J. 153 (2009) 217–221.
[39] X. Du, Y. Fang, X. Cheng, Z. Du, M. Zhou, H. Wang, Fabrication and characterization of flame-retardant nanoencapsulated n-octadecane with melamine-formaldehyde shell for thermal energy storage, ACS Sustain. Chem. Eng. 6 (2018) 15541–15549.
[40] Y. Zhu, Y. Chi, S. Liang, X. Luo, K. Chen, C. Tian, J. Wang, L. Zhang, Novel metal coated nanoencapsulated phase change materials with high thermal conductivity for thermal energy storage, Sol. Energy Mater. Sol. Cells 176 (2018) 212–221.

[41] Y. Zhu, Y. Qin, C. Wei, S. Liang, X. Luo, J. Wang, L. Zhang, Nanoencapsulated phase change materials with polymer-SiO2 hybrid shell materials: compositions, morphologies, and properties, Energy Convers. Manage. 164 (2018) 83–92.
[42] A. Zhao, J. An, J. Yang, E.-H. Yang, Microencapsulated phase change materials with composite titania-polyurea (TiO2-PUA) shell, Appl. Energy 215 (2018) 468–478.
[43] M. Ghalambaz, A. Doostani, E. Izadpanahi, A. Chamkha, Phase-change heat transfer in a cavity heated from below: the effect of utilizing single or hybrid nanoparticles as additives, J. Taiwan Inst. Chem. Eng. 72 (2017) 104–115.
[44] A. Chamkha, A. Doostanidezfuli, E. Izadpanahi, M. Ghalambaz, Phase-change heat transfer of single/hybrid nanoparticles-enhanced phase-change materials over a heated horizontal cylinder confined in a square cavity, Adv. Powder Technol. 28 (2017) 385–397.
[45] R. Elbahjaoui, H. El Qarnia, Transient behavior analysis of the melting of nanoparticle-enhanced phase change material inside a rectangular latent heat storage unit, Appl. Therm. Eng. 112 (2017) 720–738.
[46] X. Xiao, P. Zhang, M. Li, Preparation and thermal characterization of paraffin/metal foam composite phase change material, Appl. Energy 112 (2013) 1357–1366.
[47] X. Xiao, P. Zhang, M. Li, Effective thermal conductivity of open-cell metal foams impregnated with pure paraffin for latent heat storage, Int. J. Therm. Sci. 81 (2014) 94–105.
[48] B.V.S. Dinesh, A. Bhattacharya, Effect of foam geometry on heat absorption characteristics of PCM-metal foam composite thermal energy storage systems, Int. J. Heat Mass Transf. 134 (2019) 866–883.
[49] Z.-G. Wu, W.-C. Sheng, W.-Q. Tao, Z. Li, A novel experimental-numerical method for studying the thermal behaviors of phase change material in a porous cavity, Sol. Energy 169 (2018) 325–334.
[50] C.-J. Ho, J. Huang, P. Tsai, Y.M. Yang, Water-based suspensions of Al2O3 nanoparticles and MEPCM particles on convection effectiveness in a circular tube, Int. J. Therm. Sci. 50 (2011) 736–748.
[51] C.-J. Ho, W.-C. Chen, W.-M. Yan, Correlations of heat transfer effectiveness in a minichannel heat sink with water-based suspensions of Al2O3 nanoparticles and/or MEPCM particles, Int. J. Heat Mass Transf. 69 (2014) 293–299.
[52] C.-J. Ho, W.-C. Chen, W.-M. Yan, Experimental study on cooling performance of minichannel heat sink using water-based MEPCM particles, Int. Commun. Heat Mass Transf. 48 (2013) 67–72.
[53] H.R. Seyf, Z. Zhou, H. Ma, Y. Zhang, Three dimensional numerical study of heat-transfer enhancement by nano-encapsulated phase change material slurry in microtube heat sinks with tangential impingement, Int. J. Heat Mass Transf. 56 (2013) 561–573.
[54] H.R. Seyf, M.R. Wilson, Y. Zhang, H. Ma, Flow and heat transfer of nanoencapsulated phase change material slurry past a unconfined square cylinder, J. Heat Transf. 136 (2014) 051902.
[55] M. Ghalambaz, A.J. Chamkha, D. Wen, Natural convective flow and heat transfer of Nano-Encapsulated Phase Change Materials (NEPCMs) in a cavity, Int. J. Heat Mass Transf. 138 (2019) 738–749.
[56] M. Hunger, A.G. Entrop, I. Mandilaras, H. Brouwers, M. Founti, The behavior of self-compacting concrete containing micro-encapsulated phase change materials, Cem. Concr. Compos. 31 (2009) 731–743.
[57] T. Toppi, L. Mazzarella, Gypsum based composite materials with micro-encapsulated PCM: experimental correlations for thermal properties estimation on the basis of the composition, Energy Build. 57 (2013) 227–236.
[58] M. Ghalambaz, T. Groşan, I. Pop, Mixed convection boundary layer flow and heat transfer over a vertical plate embedded in a porous medium filled with a suspension of nano-encapsulated phase change materials, J. Mol. Liq. 111432 (2019).
[59] M. Ghalambaz, M.A. Sheremet, I. Pop, Free convection in a parallelogrammic porous cavity filled with a nanofluid using Tiwari and Das' nanofluid model, PLoS ONE 10 (2015) e0126486.
[60] A. Hajjar, S. Mehryan, M. Ghalambaz, Time periodic natural convection heat transfer in a nano-encapsulated phase-change suspension, Int. J. Mech. Sci. 105243 (2019).
[61] S. Mehryan, E. Izadpanahi, M. Ghalambaz, A. Chamkha, Mixed convection flow caused by an oscillating cylinder in a square cavity filled with Cu–Al 2 O 3/water hybrid nanofluid, J. Therm. Anal. Calorim. (2019) 1–18.
[62] S. Mehryan, M. Izadi, Z. Namazian, A.J. Chamkha, Natural convection of multi-walled carbon nanotube–Fe 3 O 4/water magnetic hybrid nanofluid flowing in porous medium considering the impacts of magnetic field-dependent viscosity, J. Therm. Anal. Calorim. 138 (2019) 1541–1555.
[63] M. Ghalambaz, S.H. Zadeh, S. Mehryan, I. Pop, D. Wen, Analysis of melting behavior of PCMs in a cavity subject to a line source magnetic field using a moving grid technique, Appl. Math. Model. (2019).
[64] L. Chai, R. Shaukat, L. Wang, H.S. Wang, A review on heat transfer and hydrodynamic characteristics of nano/microencapsulated phase change slurry (N/MPCS) in mini/microchannel heat sinks, Appl. Therm. Eng. 135 (2018) 334–349.
[65] B. Chen, X. Wang, R. Zeng, Y. Zhang, X. Wang, J. Niu, Y. Li, H. Di, An experimental study of convective heat transfer with microencapsulated phase change material suspension: laminar flow in a circular tube under constant heat flux, Exp. Therm Fluid Sci. 32 (2008) 1638–1646.
[66] K. Khanafer, K. Vafai, A critical synthesis of thermophysical characteristics of nanofluids, Int. J. Heat Mass Transf. 54 (2011) 4410–4428.
[67] A. Zaraki, M. Ghalambaz, A.J. Chamkha, M. Ghalambaz, D. De Rossi, Theoretical analysis of natural convection boundary layer heat and mass transfer of nanofluids: effects of size, shape and type of nanoparticles, type of base fluid and working temperature, Adv. Powder Technol. 26 (2015) 935–946.
[68] J.C. De Los Reyes, S. González Andrade, A combined BDF-semismooth Newton approach for time-dependent Bingham flow, Numer. Methods Partial Differ. Eq. 28 (2012) 834–860.
[69] O. Schenk, K. Gärtner, Solving unsymmetric sparse systems of linear equations with PARDISO, Future Gener. Comput. Syst. 20 (2004) 475–487.
[70] P. Wriggers, Nonlinear Finite Element Methods, Springer Science & Business Media, 2008.
[71] F. Verbosio, A. De Coninck, D. Kourounis, O. Schenk, Enhancing the scalability of selected inversion factorization algorithms in genomic prediction, J. Comput. Sci. 22 (2017) 99–108.
[72] K. Kahveci, Buoyancy driven heat transfer of nanofluids in a tilted enclosure, J. Heat Transf. 132 (2010) 062501.
[73] P. Nithiarasu, K. Seetharamu, T. Sundararajan, Natural convective heat transfer in a fluid saturated variable porosity medium, Int. J. Heat Mass Transf. 40 (1997) 3955–3967.
[74] E.V. Kalabin, M.V. Kanashina, P.T. Zubkov, Natural-convective heat transfer in a square cavity with time-varying side-wall temperature, Numeri. Heat Transf. Part A: Appl. 47 (2005) 621–631.